Article

Retrodeformation of the Steinheim Cranium: Insights into the Evolution of Neanderthals

Costantino Buzi [1,*] , **Antonio Profico** [2] , **Fabio Di Vincenzo** [3,4] , **Katerina Harvati** [1,5] , **Marina Melchionna** [6] , **Pasquale Raia** [6] **and Giorgio Manzi** [4,7]

1 DFG Centre for Advanced Studies 'Words, Bones, Genes, Tools', Eberhard Karls University of Tübingen, Rümelinstr. 23, 72070 Tübingen, Germany; katerina.harvati@ifu.uni-tuebingen.de
2 PalaeoHub, Department of Archaeology, University of York, King's Manor, York YO1 7EP, UK; antonio.profico@york.ac.uk
3 Natural History Museum, University of Florence, 50121 Firenze, Italy; fabio.divincenzo@unifi.it
4 Italian Institute of Human Paleontology (Is.I.P.U.), 03012 Anagni, Italy; giorgio.manzi@uniroma1.it
5 Paleoanthropology, Senckenberg Centre for Human Evolution and Palaeoenvironments, Institute for Archaeological Sciences, Eberhard Karls University of Tübingen, Rümelinstr. 23, 72070 Tübingen, Germany
6 Dipartimento di Scienze della Terra, dell'Ambiente e delle Risorse, Università di Napoli Federico II, 80138 Napoli, Italy; marina.melchionna@unina.it (M.M.); pasquale.raia@unina.it (P.R.)
7 Department of Environmental Biology, Sapienza University of Rome, 00185 Roma, Italy
* Correspondence: costantino.buzi@uni-tuebingen.de

Abstract: A number of different approaches are currently available to digitally restore the symmetry of a specimen deformed by taphonomic processes. These tools include mirroring and retrodeformation to approximate the original shape of an object by symmetrisation. Retrodeformation has the potential to return a rather faithful representation of the original shape, but its power is limited by the availability of bilateral landmarks. A recent protocol proposed by Schlager and colleagues (2018) overcomes this issue by using bilateral landmarks and curves as well as semilandmarks. Here we applied this protocol to the Middle Pleistocene human cranium from Steinheim (Germany), the holotype of an abandoned species named *Homo steinheimensis*. The peculiar morphology of this fossil, associated with the taphonomic deformation of the entire cranium and the lack of a large portion of the right side of the face, has given rise to different hypotheses over its phylogenetic position. The reconstruction presented here sheds new light on the taphonomic origin of some features observed on this crucial specimen and results in a morphology consistent with its attribution to the Neanderthal lineage.

Keywords: digital reconstruction; *Homo heidelbergensis*; *Homo neanderthalensis*; *Homo sapiens*; Middle Pleistocene humans; virtual anthropology; Europe

1. Introduction

The study of fossil specimens has been revolutionised by the foundation of modern morphometrics [1]. Symmetry is one prominent feature of biological objects, and possibly the one affected the most by taphonomic processes [2–5]. However, symmetry also offers the possibility to restore the original shapes of fossil remains that are found broken or incomplete [6,7]. This is key to the interpretation of these specimens, since taphonomic alteration affecting diagnostic features may lead to incorrect taxonomic attributions and dubious phylogenetic reconstructions [7–9]. Digital methods for the reconstruction and restoration of broken fossil remains are nowadays available thanks to an ensemble of techniques that commonly fall under the heading of 'virtual anthropology' [10–12]. Specimens can be handled in a safe, virtual environment [7] and undergo restoration protocols that can include the realignment of dislocated fragments [13–16] or the digital removal of the plaster from traditional reconstructions [8,17] without the risk of damaging the original material. These protocols can be associated with symmetrisation, which helps to

recreate missing portions or 'undo' the effects of plastic deformation. In the former case, symmetrisation 'fills the gaps' (i.e., missing portions) in one half of the fossil by mirroring the preserved counterparts [7,18–22]. In the latter case, referred to as retrodeformation, the plastic distortion of the original shape is corrected by relying on biological symmetry, as calculated by the acquisition of bilateral landmarks, curves, or patches of semiland-marks [4,7,8,23–28]. Mardia and colleagues [3] defined two types of bilateral symmetry: one referring to structures present as two separate copies on both sides of the specimen as mirror images (matching symmetry), the other defined (in three-dimensional objects) by the midsagittal plane passing through the specimen and thus determining an internal left–right symmetry (object symmetry) [2,3]. One key difference between matching and object symmetry is that genuine asymmetry is ignored by the former, but still apparent under the latter. In the case of the vertebrate skull, which provides an example of object symmetry [3], this implies that retrodeformation preserves genuine asymmetry, whereas mirroring does not. Moreover, mirroring can generate artefacts, or a biased morphology, if the only preserved portion is itself distorted [7]. On the other hand, the application of retrodeformation can be affected by the state of preservation of the object [4].

A perfect example of the combination of missing parts and plastic deformation affecting a single specimen is given by the cranium from Steinheim (hereafter, Steinheim), which is the holotype of the abandoned species *Homo steinheimensis* (Berckhemer, 1936) [29]. This human fossil was found in July 1933 in a gravel pit 70 km north of the town of Steinheim an der Murr, Baden-Württemberg, Germany [30,31] (Figure 1). It was recovered from Pleistocene fluvial deposits along the Murr river, which were well known at the time of the discovery for having yielded well-preserved fossils of Pleistocene mammals [30,32]. Since the discovery came from a well-studied area, the fossil received proper geological contextualisation. It was therefore possible to estimate the specimen's age based on the biochronological dating of the faunal assemblage, roughly corresponding to OIS 9 (i.e., 300–320 ka to 250 ka) [30,32–35].
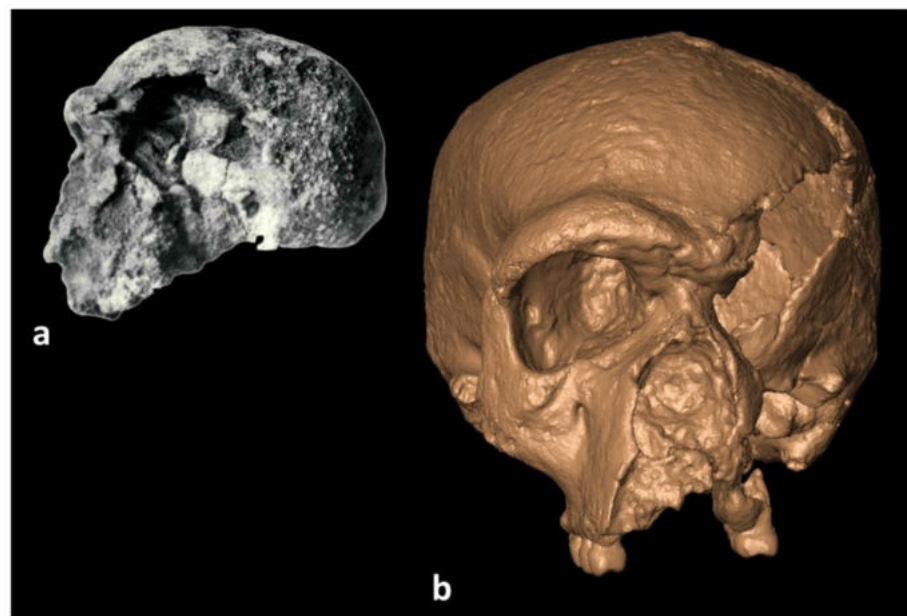
Figure 1. The cranium from Steinheim: (**a**) the cranium (left side) at the moment of recovery (from [30]); (**b**) a digital rendering of the cranium (front side).

The complex pattern of deformation that affected Steinheim, as well as its incomplete status and the presence of extensive incrustations, made it difficult to discern whether its peculiar morphology represents the original shape of the individual, or it is the product of taphonomic deformation [36,37]. This uncertainty contributed to a longstanding debate concerning the Steinheim phylogenetic position [36,38–40]. The cranium is characterised by

a peculiar mixture of archaic and derived traits, which originated different proposals about its position within or close to the Neanderthal lineage—as representing a 'pre-Neanderthal stage' along the so-called process of accretion—or even as a specimen somehow related to the origin of *Homo sapiens* [41–45]. However, not only most of the left side of the facial skeleton in Steinheim is missing, but also the cranium presents a peculiar plastic deformation, further complicating the recognition of its features. For example, the highly diagnostic infraorbital plate and orbitomaxillary region are preserved only on the left side. This part of Steinheim's face shows an angled transverse profile, which was interpreted in the past as 'anticipating' the modern human morphology to some degree [30,43], but has been conversely interpreted as the result of the retention of archaic facial morphology, also observed in some Western European earlier taxa (i.e., *Homo antecessor*) [46–48]. The relatively low and long neurocranium of Steinheim, possessing a rather vertical occipital plane, also shows a slightly angled coronal profile, or a 'roofed' appearance [36], with the maximum cranial width occurring in the lower portion [35].

A specific name was initially proposed for this specimen (*Homo steinheimensis* Bereckhemer, 1936) [29], but it is currently considered invalid [40,49], despite that this name has been resurrected at the taxonomic rank of subspecies [50,51]. Steinheim is now generally considered as belonging to the Neanderthal lineage [45,52–54] and possibly related to other Middle Pleistocene populations (e.g., Atapuerca Sima de los Huesos, SH), with which it shares several derived traits in addition to its the geographical and chronological attributions [45,53,54].

2. Materials and Methods

The description of Steinheim's morphology is influenced by the extensive deformation of the skull [32,37]. A representation of the major directions of the deformation has been obtained by observations on the CT scan of the fossil and a review of literature [32,37,55] and is shown in Figure 2.
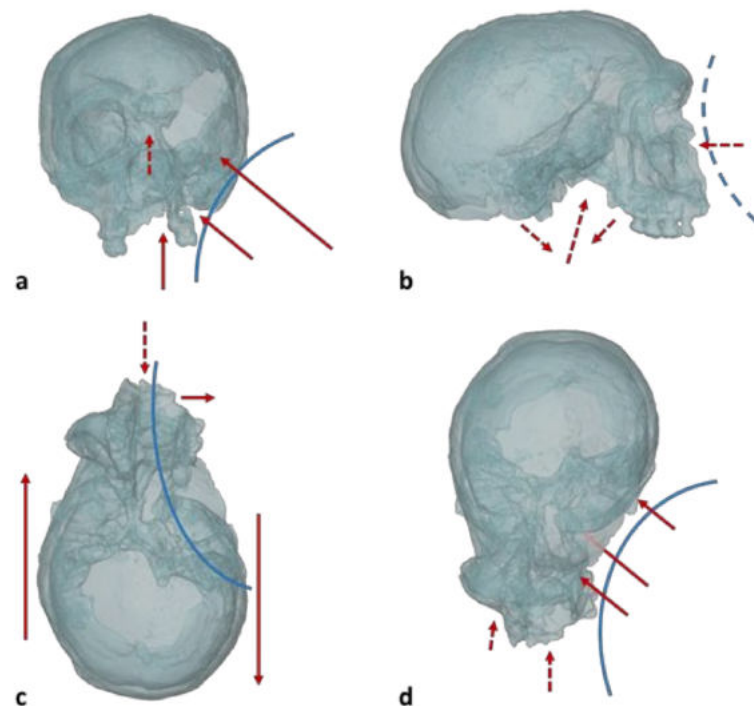
Figure 2. A simplified representation of the deformation of Steinheim. The blue lines resume the extent and area of influence of the deformation; the red arrows resume the directions of the morphological modification, associated with the areas in which the effects are visible. The solid lines point to the more evident effects of the deformation; the dashed lines represent additional possible effects. (**a**): anterior view; (**b**): right-lateral view; (**c**): inferior view; (**d**): superior view.

Prossinger and colleagues [37] performed the first digital segmentation of the cranium, resulting in a model cleared from the encrustations but still heavily affected by taphonomic distortions. Such distortions are observed in the internal structure of the cranium, including a shift to the right of the midsagittal plane of the splanchnocranium, an inward 'inflation' of the left orbital roof, and a rightward rotation of the axis of the *crista galli* in the anterior endocranial surface [37]. Since the left portion of the face is missing, it is difficult to assess how much of this morphology is determined by the deformation [37]. The right orbit is characterized by an angled shape with a sloped inferior margin. The preserved infraorbital plate shows an angled transverse profile with a point of bending roughly corresponding to the infraorbital foramen [33]. Curiously, this is associated with a moderate inflation of the anterior portion of the infraorbital plate, whereas the lateralmost portion appears flattened [35]. Through investigations conducted via CT scan and digital imaging, it was possible to assess the relative size of the frontal sinuses inside the well-developed supraorbital torus [36] and to diagnose a possible meningioma located in the upper part of the neurocranium [56].

To obtain a reconstruction consistent with object symmetry (sensu Mardia and colleagues [3]), we started by applying retrodeformation [4]. The choice of landmarks (Figure 3) was thus constrained by a criterion of symmetry: each landmark chosen on the left side must have a counterpart on the right side [4]. The incomplete state of Steinheim narrowed the choice of possible homologous landmarks and the choice of bilateral curves and surfaces for the definition of semilandmarks (Figure 3).
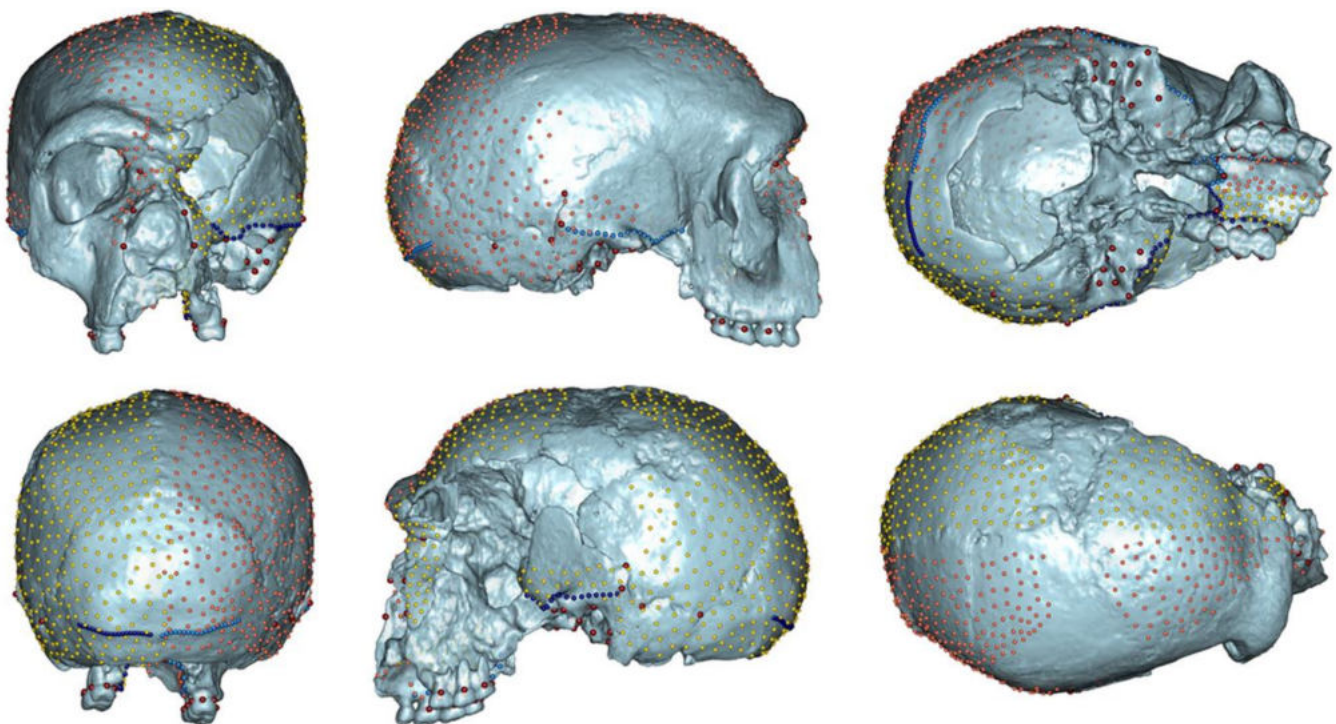

Figure 3. The configurations used: the bilateral landmarks (dark red); the bilateral curves, right (light blue) and left (dark blue); the patches of surface semilandmarks sampled on the left side (yellow) and their projection on the right side (orange).

It was possible to define only a few landmarks on the small preserved portion of the left side of the face, comprising the nasomaxillary region (Figure 3). In defining surface semilandmarks, we excluded the preserved portion of the temporal squama because it is affected by local breakage and subsequent reconstruction (see Figure 1) [36–38]. Similarly, in defining the patches of semilandmarks, the upper part of the left parietal was excluded, as this portion of the neurocranium is more affected by breakage and surface damage (Figure 3). The basioccipital is also damaged, cracked, and partly shifted inside the neurocranium itself, and therefore, no landmarks were placed on this region.

The high-resolution CT scan of Steinheim was kindly provided by Prof. Dr. Christoph P.E. Zollikofer (Department of Anthropology, University of Zurich). The CT data, obtained in the form of a DICOM stack, were processed in Amira [57] to obtain a 3D mesh, subsequently converted into the .ply format. We defined 52 bilateral landmarks on the skull and 8 curves. The curves were later processed in R by the function *equidistantCurve* (*Morpho* R package) [58] to sample evenly spaced semilandmarks along each curve. The coordinates of 500 semilandmarks were obtained by applying a *k*-means clustering algorithm to the vertex coordinates from a portion of the mesh corresponding to the left part of the cranium, from which we excluded the temporal squama and the damaged area of the coronal suture (Figure 3). The set of surface semilandmarks built this way was rotated and projected on the right side. In sum, we defined 8 curves (120 points), 52 bilateral landmarks, and 1000 surface semilandmarks for a total of 1172 paired coordinates (Figure 3). After the retrodeformation, applied according to the protocol in Schlager and colleagues [4], we calculated and visualized the local displacement between the starting and retrodeformed meshes using the function *localmeshdiff* (*Arothron* R package) [59]. The retrodeformed model of Steinheim was eventually subjected to a principal component analysis (PCA) in the shape space, together with the original model and a comparison sample including modern humans (N = 17), Neanderthals (N = 5), and Middle Pleistocene humans (N = 3). The comparison sample for the PCA is reported in Supplementary Table S1. The cranial landmark configuration used for the analysis was built upon the preserved portions of Steinheim and is figured in Supplementary Figure S1.

3. Results

3.1. The Retrodeformation

Most of the retrodeformation procedure intervened on the anteroposterior shift of the two sides of the skull (Figure 2c). In the frontal view (Figure 4a), the shift produces a relative enlargement of the piriform aperture, mainly on the left side, associated with a forward shift of the left rim and a slight retraction of the medial portion of the right rim. A slight 'relaxation' of the nasal profile in the superoinferior direction is apparent, as well as the symmetrisation of the general profile of the neurocranium, which is even more evident in the posterior view (Figure 4b). Symmetrisation of the occlusal plane of the teeth eliminates the unnatural downward displacement of the right maxilla along the midsagittal plane, which is present in the original specimen (Figure 4a,b).

The correction of the anteroposterior shift of the face along the midsagittal plane is also evident from the inferior view (Figure 4c), where the reduction of the slight clockwise rotation of the palate becomes apparent, accompanied by a deflation of the right postorbital portion of the neurocranium. In addition, the basicranium regained a more natural position, appearing straighter and medially placed in comparison with the original specimen, even though a slight deformation remains due to the lack of landmarks to be placed on this badly preserved portion. Preservation similarly affects the retrodeformation process of the flexion of the basicranium and the anteroposterior compression along the coronal suture (Figure 4d). In the lateral view (Figure 4d), the general profile of the neurocranium does not show any major changes. However, it is evident that the retrodeformation produces a retraction of the right portion of the face. Corresponding to the frontal squama, it is possible to see in transparency the previous position of the right side (Figure 4d), which was originally shifted forward according to the deformation directions illustrated in Figure 2.

3.2. Local Displacement

The local displacement between the starting and the retrodeformed meshes (Figure 5) indicates the areas of maximum expansion, which is apparent on almost the entire left side of the skull, with the highest values recorded in the preserved portions of the left maxilla, left parietal, and left orbit. Conversely, the right side of the face is affected almost entirely by contraction, with the highest values recorded at the level of the anterior portion of the maxilla and nasofrontal suture. However, the inferior portion of the right maxilla is

expanded in the retrodeformed mesh. A somewhat balanced pattern of deformation occurs on the basicranium. The areas of maximum contraction on the right side are associated with areas of maximum expansion on the opposite side. Similarly, the moderate expansion recorded on the right side of the occipital squama corresponds to an almost symmetrical contraction of the left side. Lastly, along the midsagittal plane an area of contraction appears evident.
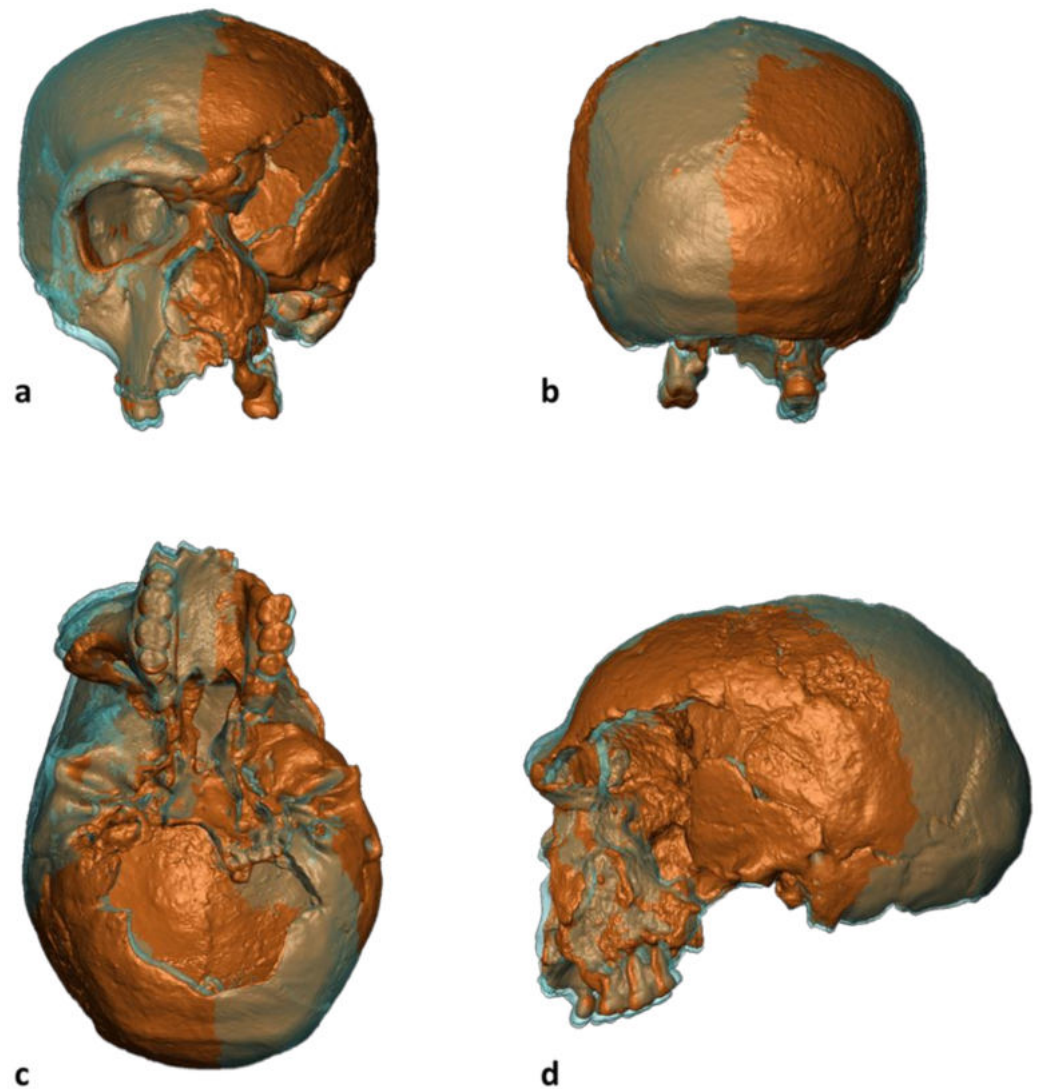

Figure 4. Comparison between the retrodeformed model of Steinheim (brown) and the original specimen (transparent blue). (**a**): anterior view; (**b**): posterior view; (**c**): inferior view; (**d**): left-lateral view.

3.3. Principal Component Analysis

The results of the PCA are reported in Figure 6. The first three PCs explain 62.74% of the total variance in the sample, weighting 41.51%, 12.27% and 8.96%, respectively. In the plot, it is possible to discern a clear separation between modern (*Sap*) and fossil humans both along PC1 and PC3. Along PC2 is visible the separation between the Neanderthals sensu stricto (*Nea*) and a small group of Middle Pleistocene humans (*Mph*). The two models of Steinheim (*Ste*) fall within an intermediate position along PC1, between the *Sap* cluster and the fossil human group. While the original model of Steinheim (*Ori*) clearly diverges from the rest of the sample along both PC1 and PC2, the retrodeformed model of Steinheim (*R.D.*) approaches the fossil human group along the PC1, reaching the limit of the *Nea* cluster along PC2.
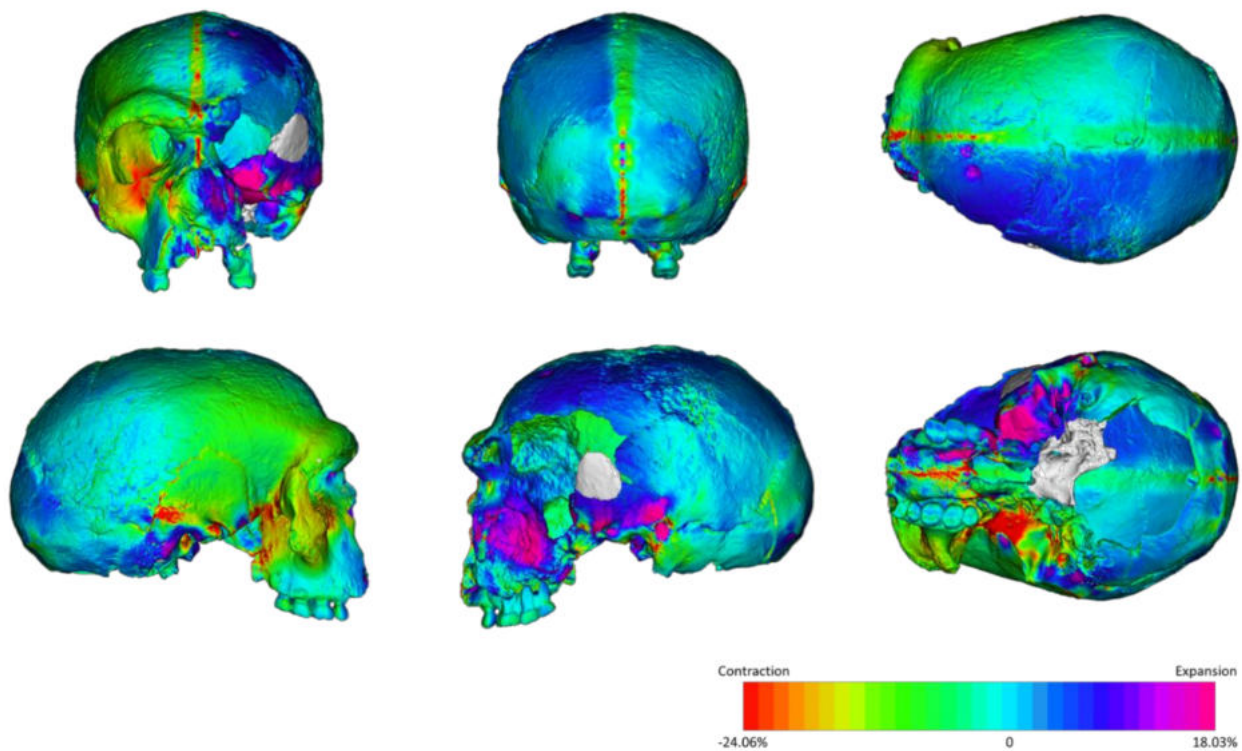
Figure 5. Local displacement (%) in the retrodeformed model of Steinheim, calculated by the function *localmeshdiff*. The white areas represent heavily damaged (basioccipital) or reconstructed (left temporal) portions of the skull that were excluded from this analysis.
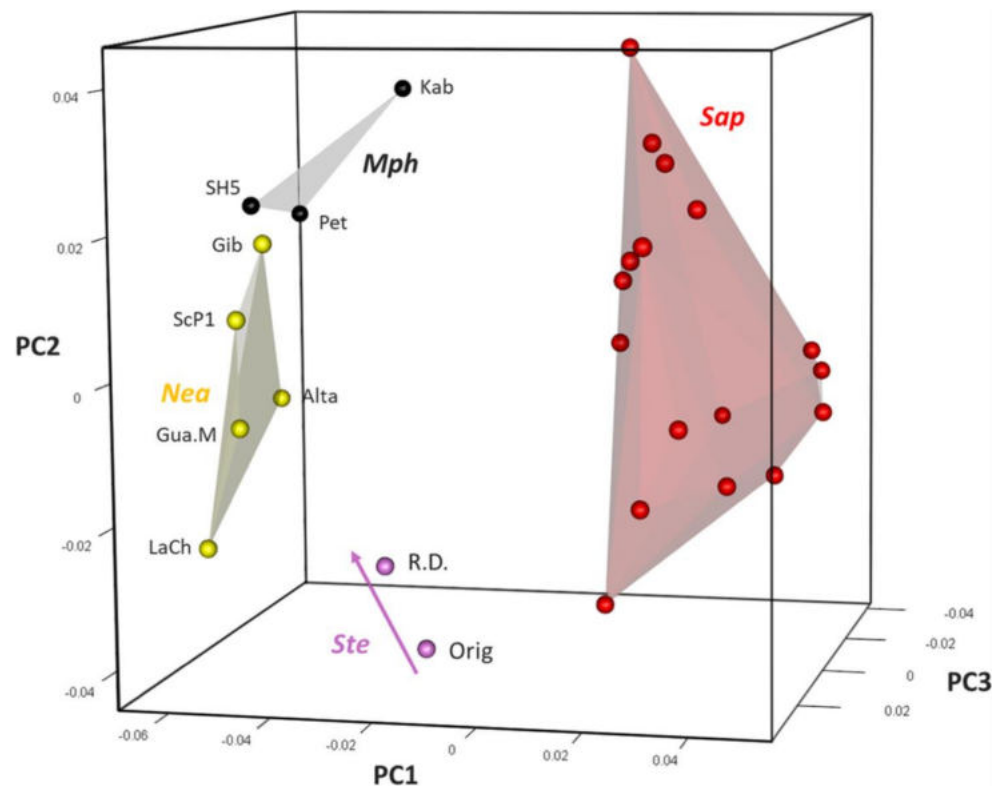

Figure 6. Shape PCA on cranial landmark configuration. In black, Middle Pleistocene humans (*Mph*); in yellow, Neanderthals (*Nea*); in red, modern humans (*Sap*); in violet, Steinheim (*Ste*): original model (*Ori*) and retrodeformed model (*R.D.*). The abbreviations of the fossil samples are reported in Supplementary Table S1.

4. Discussion

We used a retrodeformation protocol to produce a restoration of the Steinheim cranium. The application seemingly restored object symmetry to the specimen [3], despite the poor starting conditions of this incomplete and severely deformed fossil. We relied on the preserved portions, mainly on the left side of the cranium, to drive the reshaping of its counterpart. Even though some directions of the taphonomic deformations were not addressed, our application minimises their effect. The reconstruction (Figure 7), hence, allows us to better contextualise Steinheim among the coeval—or at least chronologically close—Middle Pleistocene *Homo* specimens. The neurocranial shape in the posterior view appears intermediate in morphology between the populations of Sima de los Huesos and early Neanderthals (e.g., Saccopastore 1), in keeping with the slight lateral expansion of the parietal walls after the reconstruction as compared with the more vertical and 'compressed' profile in *Ori*. In this respect, the neurocranial morphology of *R.D.* seems to approach the morphology of the early Neanderthal from Altamura [60]. In the posterior view, the original 'roofed' appearance (as described by Schwartz and Tattersall [36]) weakens in *R.D.* neurocranium, appearing close in morphology to penecontemporaneous individuals such as Skull SH5 from Atapuerca [40,54,61], except for the further laterolateral enlargement of the parietals. This trait, difficult to discern before restoring symmetry, places the maximum width of the skull in a slightly lower position relative to that of the original specimen, and roughly at the level of the temporal squama, similar to the typical Neanderthal condition [62] (Figure 4a,b). It is also possible to see a change in the relative position of the two mastoid processes, which, although partly damaged, after retrodeformation show reduced development compared with those of SH5. Their slight rotation can be interpreted as a trait anticipating the Neanderthal condition of tapering [44,45,62], although high variability in this feature among the Middle Pleistocene humans has been observed [63].
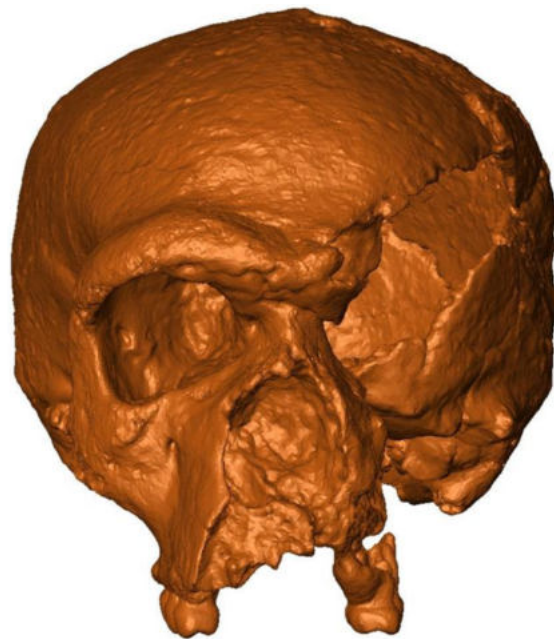

Figure 7. The retrodeformed model of Steinheim.

An almost symmetrical pattern of contraction and expansion is visible at the level of the glenoid fossae (Figure 5), associated with a change in the relative size of the postorbital portion of the neurocranium. This contributes, in turn, to the slight shortening and latero-lateral enlargement of the neurocranium. On the other hand, the 'strip' recorded along the midsagittal axis (Figure 5) corresponds to an almost continuous area of contraction, which is a clear indication of the taphonomic deformation that occurred along this axis

(see Figure 2c). This 'strip' can probably be traced back to a local expansion along the midsagittal line due to the two 'halves' moving in opposite directions.

As can be seen from Figure 5, the retrodeformation was not able to address the anteroposterior vectors of deformation. This is because such vectors acted in a single straight line, rather than bilaterally. Thus, it is not possible to reach evidence-based assumptions on whether the flexion of the basicranium reflects the original condition or it is the result of taphonomic deformation. Nevertheless, the restored midsagittal profile of the cranium suggests that the anteroposteriorly elongated profile of the neurocranium could possibly be associated with a less flexed basicranium. As we proposed in Figure 2b, the present flexion could be related to a deformation operating along the sagittal axis on the upper midface.

Unfortunately, the almost completely missing left portion of the face made it difficult to correct for some local modifications in this area. Nonetheless, it is still possible to carefully evaluate whether some features are due to taphonomic deformation. As mentioned above, the retrodeformation resulted in a 'proper' midsagittal profile (Figure 4d) by undoing the rotational deformation caused by the anterolateral crushing (Figure 2d). By examining the lateral view of the reconstruction, it is more evident how the 'plica' obliterating the frontonasal suture—which is not found in any other hominin from Middle to Late Pleistocene—is consistent with an anterior crushing of the upper part of the nasal portion (Figure 2a). This, in turn, can be associated with the 'notch' found along the lower-right orbital rim, corresponding to a point of weakness represented by the zygomaxillary suture. We suggest that the peculiar facial morphology of Steinheim is mostly a result of the crushing that occurred in the upper portion of the midface (Figure 2b). In our opinion, the reconstruction showed that the infraorbital plate was in origin possibly less flexed than *Ori* suggests.

As evidenced by the PCA (Figure 6), Steinheim is distinguished from the rest of the sample, and this 'uniqueness' can be traced back to its complex pattern of taphonomic deformation. Nonetheless, when a part of this is corrected by retrodeformation, it is possible to see how the new model approaches the fossil human subsample, towards the Neanderthal cluster. We hypothesize that since some of the deformation vectors—namely, those operating on the anteroposterior axis—cannot be intercepted by the retrodeformation, Steinheim still presents itself with a 'unique' morphology, distinguished from other Middle Pleistocene specimens.

5. Conclusions

The 'mosaic' evolution of the typical Neanderthal cranial morphology (i.e., 'classic' Neanderthal cranial shape [62]) seems to have included an earlier development of some facial traits, combined with the retention of a more primitive condition for the neurocranium [51,61]. The full development of the typical Neanderthal *en-bombe* shape must thus be considered a derived trait. Consequently, the moderate expansion of the parietals of the retrodeformed Steinheim (posterior view, Figure 4b) suggests association with a greater expression of midfacial prognathism than that observed in this individual, consistent with other specimens from the Middle Pleistocene of Europe. In our opinion, the present facial morphology of Steinheim is influenced by the deformation caused on the upper midface by taphonomy. Even though the reconstruction presented here did not correct the whole pattern of deformation, nor did it provide the exact original shape of Steinheim, it contributes to shedding new light on the morphology of this specimen and concurrently to placing Steinheim more firmly in the Neanderthal evolutionary lineage.

References

1. Bookstein, F.L. The study of shape transformation after D'Arcy Thompson. *Math. Biosci.* **1977**, *34*, 177–219. [CrossRef]
2. Klingenberg, C.P.; Barluenga, M.; Meyer, A. Shape analysis of symmetric structures: Quantifying variation among individuals and asymmetry. *Evolution* **2002**, *56*, 1909–1920. [CrossRef]
3. Mardia, K.V.; Bookstein, F.L.; Moreton, I.J. Statistical assessment of bilateral symmetry of shapes. *Biometrika* **2000**, *87*, 285–300. [CrossRef]
4. Schlager, S.; Profico, A.; Di Vincenzo, F.; Manzi, G. Retrodeformation of fossil specimens based on 3D bilateral semi-landmarks: Implementation in the R package "Morpho". *PLoS ONE* **2018**, *13*, e0194073. [CrossRef]
5. Fernández-Jalvo, Y.; Andrews, P. *Atlas of Taphonomic Identifications*; Springer: Dordrecht, The Netherlands, 2016; p. 4.
6. Adams, D.C.; Rohlf, F.J.; Slice, D.E. A field comes of age: Geometric morphometrics in the 21st century. *Hystrix* **2013**, *24*, 7–14.
7. Gunz, P.; Mitteroecker, P.; Neubauer, S.; Weber, G.W.; Bookstein, F.L. Principles for the virtual reconstruction of hominin crania. *J. Hum. Evol.* **2009**, *57*, 48–62. [CrossRef]
8. Di Vincenzo, F.; Profico, A.; Bernardini, F.; Cerroni, V.; Dreossi, D.; Schlager, S.; Zaio, P.; Benazzi, S.; Biddittu, I.; Rubini, M.; et al. Digital reconstruction of the Ceprano calvarium (Italy), and implications for its interpretation. *Sci. Rep.* **2017**, *7*, 1–11. [CrossRef]
9. White, T. Early hominids—Diversity or distortion? *Science* **2003**, *299*, 1994–1997. [CrossRef]
10. Weber, G.W.; Schäfer, K.; Prossinger, H.; Gunz, P.; Mitteröcker, P.; Seidler, H. Virtual anthropology: The digital evolution in anthropological sciences. *J. Physiol. Anthropol. Appl. Human Sci.* **2001**, *20*, 69–80. [CrossRef]
11. Weber, G.W. Another link between archaeology and anthropology: Virtual anthropology. *DAACH* **2014**, *1*, 3–11. [CrossRef]
12. Weber, G.W. Virtual anthropology. *Am. J. Phys. Anthropol.* **2015**, *156*, 22–42. [CrossRef]
13. Amano, H.; Kikuchi, T.; Morita, Y.; Kondo, O.; Suzuki, H.; Ponce de León, M.S.; Zollikofer, C.P.E.; Bastir, M.; Stringer, C.B.; Ogihara, N. Virtual reconstruction of the Neanderthal Amud 1 cranium. *Am. J. Phys. Anthropol.* **2015**, *158*, 185–197. [CrossRef] [PubMed]
14. Bosman, A.M.; Buck, L.T.; Reyes-Centeno, H.; Mirazón Lahr, M.; Stringer, C.B.; Harvati, K. The Kabua 1 cranium: Virtual anatomical reconstructions. In *Modern Human Origins and Dispersal*; Sahle, Y., Reyes-Centeno, H., Bentz, C., Eds.; Kerns Verlag: Tübingen, Germany, 2019; pp. 137–170.
15. Harvati, K.; Röding, C.; Bosman, A.M.; Karakostis, F.A.; Grün, R.; Stringer, C.B.; Karkanas, P.; Thompson, N.C.; Koutoulidis, V.; Moulopoulos, L.A.; et al. Apidima Cave fossils provide earliest evidence of *Homo sapiens* in Eurasia. *Nature* **2019**, *571*, 500–504. [CrossRef]
16. Profico, A.; Buzi, C.; Davis, C.; Melchionna, M.; Veneziano, A.; Raia, P.; Manzi, G. A new tool for digital alignment in virtual anthropology. *Anat. Rec.* **2019**, *302*, 1104–1115. [CrossRef] [PubMed]
17. Benazzi, S.; Bookstein, F.L.; Strait, D.S.; Weber, G.W. A new OH5 reconstruction with an assessment of its uncertainty. *J. Hum. Evol.* **2011**, *61*, 75–88. [CrossRef] [PubMed]
18. Benazzi, S.; Gruppioni, G.; Strait, D.S.; Hublin, J.J. Virtual reconstruction of KNM-ER 1813 *Homo habilis* cranium. *Am. J. Phys. Anthropol.* **2014**, *153*, 154–160. [CrossRef] [PubMed]
19. Berge, C.; Goularas, D. A new reconstruction of Sts 14 pelvis (*Australopithecus africanus*) from computed tomography and three-dimensional modeling techniques. *J. Hum. Evol.* **2010**, *58*, 262–272. [CrossRef]
20. Gunz, P.; Neubauer, S.; Golovanova, L.; Doronichev, V.; Maureille, B.; Hublin, J.J. A uniquely modern human pattern of endocranial development. Insights from a new cranial reconstruction of the Neandertal newborn from Mezmaiskaya. *J. Hum. Evol.* **2012**, *62*, 300–313. [CrossRef]
21. Hublin, J.J.; Ben-Ncer, A.; Bailey, S.E.; Freidline, S.E.; Neubauer, S.; Skinner, M.M.; Bergmann, I.; Le Cabec, A.; Benazzi, S.; Harvati, K.; et al. New fossils from Jebel Irhoud, Morocco and the pan-African origin of *Homo sapiens*. *Nature* **2017**, *546*, 289–292. [CrossRef]

22. Vialet, A.; Guipert, G.; Alçiçek, M.C. *Homo erectus* found still further west: Reconstruction of the Kocabaş cranium (Denizli, Turkey). *Comptes Rendus Palevol.* **2012**, *11*, 89–95. [CrossRef]

23. Arbour, V.M.; Currie, P.J. Analyzing taphonomic deformation of ankylosaur skulls using retrodeformation and finite element analysis. *PLoS ONE* **2012**, *7*, e39323. [CrossRef] [PubMed]

24. Kazhdan, M.M.; Amenta, N.; Gu, S.; Wiley, D.F.; Hamann, B. Symmetry restoration by stretching. In Proceedings of the 21st Canadian Conference on Computational Geometry (CCCG2009), Vancouver, Canada, 17–19 August 2009; CCCG: Vancouver, BC, Canada, 2009; pp. 37–40.

25. Lautenschlager, S. Reconstructing the past: Methods and techniques for the digital restoration of fossils. *Roy. Soc. Open Sci.* **2016**, *3*, 160342. [CrossRef]

26. Ogihara, N.; Nakatsukasa, M.; Nakano, Y.; Ishida, H. Computerized restoration of nonhomogeneous deformation of a fossil cranium based on bilateral symmetry. *Am. J. Phys. Anthropol.* **2006**, *130*, 1–9. [CrossRef]

27. Tallman, M.; Amenta, N.; Delson, E.; Frost, S.R.; Ghosh, D.; Klukkert, Z.S.; Morrow, A.; Sawyer, G.J. Evaluation of a new method of fossil retrodeformation by algorithmic symmetrization: Crania of papionins (Primates, Cercopithecidae) as a test case. *PLoS ONE* **2014**, *9*, e100833. [CrossRef]

28. Tschopp, E.; Russo, J.; Dzemski, G. Retrodeformation as a test for the validity of phylogenetic characters: An example from diplodocid sauropod vertebrae. *Palaeontol. Electron.* **2016**, *16*, 2T. [CrossRef]

29. Berckhemer, F. Der Urmenschenschädel aus den zwischeneiszeitlichen Fluss-Schottern von Steinheim an der Murr. *Forsch u Fortschr* **1936**, *12*, 349–350.

30. Adam, K.D. The chronological and systematic position of the Steinheim skull. In *Ancestors: The Hard Evidence*; Delson, E., Ed.; Liss: New York, NY, USA, 1985; pp. 272–276.

31. Granat, J.; Peyre, É. L'énigme odontologique du crâne de Steinheim 280 ka-Allemagne. *Actes SFHAD* **2008**, *13*, 14–18.

32. Wahl, J.; König, H.; Ziegler, R. Die Defekt-und Verformungsspuren am Schädel des Urmenschen von Steinheim an der Murr. *Fundber. Baden-Württ.* **2009**, *30*, 7–28.

33. Weinert, H. Der urmenschenschädel von Steinheim. *Z. Morphol. Anthropol.* **1936**, *35*, 463–518.

34. Czarnetzki, A. Steinheim skull: A morphological comparison with Tautavel Man. In Proceedings of the L'Homo Erectus et la Place de l'homme de Tautavel Parmi les Hominidés Fossiles, Actes Congrès International de Paléontologie Humaine, Nice, France, 16–21 October 1982; de Lumley, H., de Lumley, M.A., Eds.; pp. 875–893.

35. Street, M.; Terberger, T.; Orschiedt, J. A critical review of the German Paleolithic hominin record. *J. Hum. Evol.* **2006**, *51*, 551–579. [CrossRef] [PubMed]

36. Schwartz, J.H.; Tattersall, I. *The Human Fossil Record. Vol. 1: Terminology and Craniodental Morphology of Genus Homo (Europe)*; Wiley-Liss: New York, NY, USA, 2002; pp. 347–351.

37. Prossinger, H.; Seidler, H.; Wicke, L.; Weaver, D.; Recheis, W.; Stringer, C.B.; Müller, G.B. Electronic removal of encrustations inside the Steinheim cranium reveals paranasal sinus features and deformations and provides a revised endocranial volume estimate. *Anat. Rec. B* **2013**, *273*, 132–142. [CrossRef]

38. Wolpoff, M.H. Cranial remains of middle Pleistocene European hominids. *J. Hum. Evol.* **1980**, *9*, 339–358. [CrossRef]

39. Stringer, C.B.; Hublin, J.J.; Vandermeersch, B. The origin of anatomically modern humans in Western Europe. In *The Origins of Modern Humans: A World Survey of the Fossil Evidence*; Smith, F.H., Spencer, F., Eds.; Liss: New York, NY, USA, 1984; pp. 51–135.

40. Arsuaga, J.L.; Martinón-Torres, M.; Santos, E. *Homo steinheimensis*, a comparison between the Steinheim skull and the Atapuerca Sima de los Huesos fossils. In Proceedings of the European Society for the study of Human Evolution (ESHE) 8, Liège, Belgium, 19–21 September 2019; ESHE: Liège, Belgium, 2019; p. 7.

41. Sergi, S. The palaeanthropi in Italy: The fossil men of Saccopastore and Circeo. Part II: Discussion and interpretation. *Man* **1948**, *48*, 76–79. [CrossRef]

42. Vlček, E. A new discovery of *Homo erectus* in Central Europe. *J. Hum. Evol.* **1978**, *7*, 239–251. [CrossRef]

43. Day, M.H. *Guide to Fossil Man*, 4th ed.; University of Chicago Press: Chicago, IL, USA, 1986.

44. Dean, D.; Hublin, J.J.; Holloway, R.; Ziegler, R. On the phylogenetic position of the pre-Neandertal specimen from Reilingen, Germany. *J. Hum. Evol.* **1998**, *34*, 485–508. [CrossRef] [PubMed]

45. Hublin, J.J. The origin of Neandertals. *Proc. Natl. Acad. Sci. USA* **1998**, *106*, 16022–16027. [CrossRef] [PubMed]

46. Bermúdez de Castro, J.M.; Arsuaga, J.L.; Carbonell, E.; Rosas, A.; Martınez, I.; Mosquera, M. A hominid from the Lower Pleistocene of Atapuerca, Spain: Possible ancestor to Neandertals and modern humans. *Science* **1997**, *276*, 1392–1395. [CrossRef]

47. Freidline, S.E.; Gunz, P.; Harvati, K.; Hublin, J.J. Evaluating developmental shape changes in *Homo antecessor* subadult facial morphology. *J. Hum. Evol.* **2013**, *65*, 404–423. [CrossRef]

48. Trafí, F.R.; Bartual, M.G.; Wang, Q. The affinities of *Homo antecessor*—A review of craniofacial features and their taxonomic validity. *Anthropol. Rev.* **2018**, *81*, 225–251. [CrossRef]

49. Stringer, C. The status of *Homo heidelbergensis* (Schoetensack 1908). *Evol. Anthropol.* **2012**, *21*, 101–107. [CrossRef]

50. Manzi, G. Humans of the Middle Pleistocene: The controversial calvarium from Ceprano (Italy) and its significance for the origin and variability of *Homo heidelbergensis*. *Quat. Int.* **2016**, *411*, 254–261. [CrossRef]

51. Manzi, G. Before the emergence of *Homo sapiens*: Overview on the Early-to-Middle Pleistocene fossil record (with a proposal about *Homo heidelbergensis* at the subspecific level). *Int. J. Evol. Biol.* **2011**, *2011*, 582678. [CrossRef]

52. Stringer, C.B. Secrets of the Pit of the Bones. *Nature* **1993**, *362*, 501–502. [CrossRef]

53. Tattersall, I. Before the Neanderthals: Hominid Evolution in Middle Pleistocene Europe. In *Continuity and Discontinuity in the Peopling of Europe*; Condemi, S., Weniger, G.C., Eds.; Springer: Dordrecht, The Netherlands, 2011; pp. 47–53.

54. Mounier, A.; Caparrós, M. The phylogenetic status of *Homo heidelbergensis*—A cladistic study of Middle Pleistocene hominins. *Bull. Mém. Soc. Anthropol. Paris* **2015**, *27*, 110–134. [CrossRef]

55. Braun, M.; Hublin, J.J.; Bouchet, P. New reconstruction of the Middle Pleistocene skull of Steinheim (Baden-Würtemberg, Germany). *Am. J. Phys. Anthropol.* **1998**, *S26*, 113.

56. Czarnetzki, A.; Schwaderer, E.; Pusch, C.M. Fossil record of meningioma. *Lancet* **2003**, *362*, 408. [CrossRef]

57. Stalling, D.; Westerhoff, M.; Hege, H.C. Amira: A highly interactive system for visual data analysis. In *The Visualization Handbook*; Hansen, C., Johnson, C., Eds.; Elsevier: Amsterdam, The Netherlands, 2005; pp. 749–767.

58. Schlager, S. Morpho and Rvcg—Shape Analysis in R: R-Packages for geometric morphometrics, shape analysis and surface manipulations. In *Statistical Shape and Deformation Analysis*; Zheng, G., Li, S., Székely, G., Eds.; Academic Press: London, UK, 2017; pp. 217–256.

59. Profico, A.; Buzi, C.; Castiglione, S.; Melchionna, M.; Piras, P.; Veneziano, A.; Raia, P. Arothron: An R package for geometric morphometric methods and virtual anthropology applications. *Am. J. Phys. Anthropol.* **2021**, *176*, 144–151.

60. Buzi, C.; Di Vincenzo, F.; Profico, A.; Manzi, G. The pre-modern human fossil record in Italy from the Middle to the Late Pleistocene: An updated reappraisal. *Alp. Mediterr. Quat.* **2021**, *34*, 1–16.

61. Arsuaga, J.L.; Martínez, I.; Arnold, L.J.; Aranburu, A.; Gracia-Téllez, A.; Sharp, W.D.; Quam, R.M.; Falguères, C.; Pantoja-Pérez, A.; Bischoff, J.; et al. Neandertal roots: Cranial and chronological evidence from Sima de los Huesos. *Science* **2014**, *344*, 1358–1363. [CrossRef]

62. Churchill, S.E. *Thin on the Ground: Neandertal Biology, Archeology and Ecology*; Wiley: Hoboken, NJ, USA, 2014; pp. 15–22.

63. Harvati, K.; Hublin, J.J.; Gunz, P. Evolution of middle-late Pleistocene human cranio-facial form: A 3-D approach. *J. Hum. Evol.* **2010**, *59*, 445–464. [CrossRef]